# Pathways for Electron Transfer at MgO-Water Interfaces from *Ab Initio* Molecular Dynamics

Zhutian Ding, Zachary K. Goldsmith, and Annabella Selloni*

*Department of Chemistry, Princeton University, Princeton, New Jersey 08544, United States*

E-mail: aselloni@princeton.edu

Phone: 609-258-3837

**Abstract**

The nature of electron transfer across metal oxide-water interfaces depends significantly on the band gap of the oxide and its band edge energies relative to the potentials of relevant aqueous redox couples. Here we focus on the water interface with MgO, a prototypical wide band gap oxide whose conduction band edge is close in energy to that of water. We investigate the behavior of an excess electron at and out of equilibrium near the interface using *ab initio* molecular dynamics based on hybrid density functional theory. Our simulations show that under equilibrium conditions the excess electron (donated by an Al impurity in MgO) localizes to a mid-gap defect state comparable in energy and shape to a hydrated electron in bulk water. To characterize the electron transfer from the conduction band of MgO to interfacial product states, we dope near-equilibrium configurations of the pristine MgO-water system with Al and run short trajectories of these instantaneously out-of-equilibrium systems. We observe two distinct products associated with the excess electron: a surface-localized electron ($e^-_{surf}$) and an aqueous hydrogen radical ($H^\bullet$). The $H^\bullet$ pathway exhibits much higher activation barrier despite being more exoergic, making $e^-_{surf}$ the kinetic product. Our

characterization of the pathways on the basis of Marcus theory is consistent with the poor observed utility of MgO for water radiolysis. Moreover, we anticipate that the computational framework employed here will be broadly applicable to assessing electron transfer mechanisms at aqueous, photocatalytic interfaces.

# Introduction

Electron transfer (ET) across metal oxide-water interfaces is of great relevance in fundamental and technological applications, ranging from photocatalysis for water splitting and the photo-oxidation of organic pollutants[1,2] to radiation chemistry, where the interfacial transfer of radiolytically generated electrons in oxide materials can strongly affect the amount of $H_2$ produced during water hydrolysis.[3–7] Two important quantities that influence interfacial ET processes are the band gap ($E_g$) of the oxide material and its band edge energies relative to the potentials associated with relevant aqueous redox couples such as $H_2/H_2O$ and $H_2O/O_2$. For example, ET coupled with proton transfer may lead to the formation of hydroxyl radicals ($OH^\bullet$) at the aqueous interface of $TiO_2$, a widely used photocatalyst with $E_g$ of 3 eV and a conduction band minimum (CBM) slightly above the water reduction potential (zero of the standard hydrogen electrode, SHE).[1,2] On the other hand, hydrated electrons ($e^-_{aq}$) and H radicals ($H^\bullet$), two strongly reducing species, are typical products of ET at the water interface with wide band gap oxides (WGOs) such as $SiO_2$, $Al_2O_3$, MgO and $ZrO_2$, whose CBMs are well above the water reduction potential and relatively close to the CBM of water.[3,4,6] Hydrated electrons observed at the interfaces of these WGOs following photoexcitation, often assumed to behave as hot electrons, are known to be solvated within 1 ps.[8–10] This ultrafast timescale for solvation may in fact inhibit ET to solution by localizing the electron in a metastable, mid-gap defect state. Understanding the detailed mechanisms of ET and its relation to $H_2$ production in the latter systems would be very valuable to the field of radiation chemistry and of considerable interest for the general theory of ET processes at heterogeneous interfaces.

Fundamental studies of ET at water-WGO interfaces have been rather scarce, however, and ET mechanisms are not yet well understood given the ultrafast nature of these reactions and metastability of their intermediates.[8] DFT studies have just recently begun to unravel the energetics and interfacial hydration structures of radiolytic species at interfaces of aluminum (oxy)hydroxides,[11,12] WGO systems similarly relevant to managing radioactive waste. While equilibrium hydration structures and dynamics of MgO[13–15] and $ZrO_2$[16] have been elucidated, mechanistic and dynamical studies of ET across semiconducting oxide-water interfaces have largely focused on nanoparticles and/or candidates for solar photocatalysis such as $TiO_2$.[17–25] Such studies have nonetheless demonstrated that the interplay between electronic energy levels and water dynamics govern interfacial charge transfer[23,24,26]

In this work we aim to obtain insight into ET mechanisms at WGO-water interfaces through hybrid density functional theory (DFT) based simulations coupled with a Marcus theory-based analysis of the ET pathways. We specifically focus on the water interface with the most abundant (001) surface of MgO as a model system with relatively simple and well-characterized structural and electronic properties.[27] MgO is an ionic oxide with $E_g$ around 7.8 eV and electron affinity of 1 eV or less. Thus, the CBM is above the adiabatic redox levels $E^o(H_2O|e^-_{aq}) = -2.9\ V_{NHE}$ and $E^o(H^+|H^\bullet) = -2.3\ V_{NHE}$ of $e^-_{aq}$ and $H^\bullet$ in water (corresponding to $\sim$ -1.6 and -2.2 eV relative to the vacuum level, respectively), suggesting that an excess (e.g. radiolytically generated) electron in MgO could easily transfer to, or react with, interfacial water to form various product species. As in previous studies, we introduced an excess electron in the oxide by substituting a lattice atom (here Mg) with a donor impurity (Al), and modeled the water-MgO (001) interface by confining explicit water at the experimental density between periodically repeated MgO slabs.[14,28] We then simulated the water-oxide system using *ab initio* molecular dynamics (AIMD) to characterize the excess electron at the interface both at and out of equilibrium.

Our out-of-equilibrium simulations revealed two distinct pathways for electron transfer from MgO to the aqueous phase, both of which we analyzed on the basis of Marcus theory. One pathway resulted in the formation of a surface solvated electron, denoted $e^-_{surf}$, with an energy inside the band gap and a very small free energy barrier to activation. In contrast, a second pathway led to the formation of a hydrogen radical, denoted $H^\bullet$, with an electronic energy below the valence band maximum. This pathway was found to be thermodynamically favorable but exhibited a large free energy of activation. These findings together provide insights into the mechanism of radiolysis on MgO and similar wide band gap oxides and more broadly demonstrate fundamental principles for evaluating aqueous, interfacial photocatalysis.

# Results and Discussion

## Equilibrium Properties of the Aqueous Interface of Doped MgO

We simulated the doped MgO-water system with interatomic forces determined at the hybrid DFT level augmented with van der Waals (vdW) dispersion corrections. This level of theory is essential for reducing the self-interaction error of standard DFT, as required for a proper description of localized electronic states.[29] Although recent studies have shown that self-interaction corrections for anions and excess electrons in water can give results of higher quality compared to hybrid functionals when used properly,[30,31] here we used an exact exchange fraction $\alpha = 0.40$ that was reported to well describe the band gap of water and the energy levels of the hydrated electron[32] (see computational details in Supporting Information, SI). We also note that while AIMD propagates on an adiabatic potential energy surface, it has been proven to provide a qualitatively correct picture of the trapping dynamics of excess electrons in water and various metal oxides in previous studies.[26,32–34]

The structure and electronic properties of the aqueous interface are summarized in Figure 1, in which results for the surface in vacuum are also presented for reference. Because steps are common defects on MgO(001) surfaces,[27] we focus on a "stepped surface" model represented by a slab with one flat and one stepped surface; results for slabs with both flat or stepped surfaces are similar, as reported in Figure S2 of the Supporting Information. The known hygroscopicity of the MgO (001) surface[35] is well reproduced by AIMD simulations that show the presence of a densely packed hydration layer of mixed molecular and dissociated adsorbed molecules at the interface (Figure 1c).[13,14] The void that is seen in the water region above the hydration layer is a fluctuating feature that is consequence of the formation of this high density layer,[14] as also illustrated by the water density profile in Figure S3. However, the interfacial ET processes discussed below occurred in the high density hydration layers which we understand to be well described herein. First principles simulations of water on pristine MgO have further identified the presence of hydroxide ions slightly above the surface-bound water layer at the interface.[14,36] Their formation is attributed to the strong basicity of the MgO surface which tends to abstract protons from water, leaving hydroxide anions at the interface as a compensating electrical double layer. We found this feature of the interfacial water structure to remain essentially unaltered on the Al-doped MgO surface, despite the presence of the excess electron at the interface.

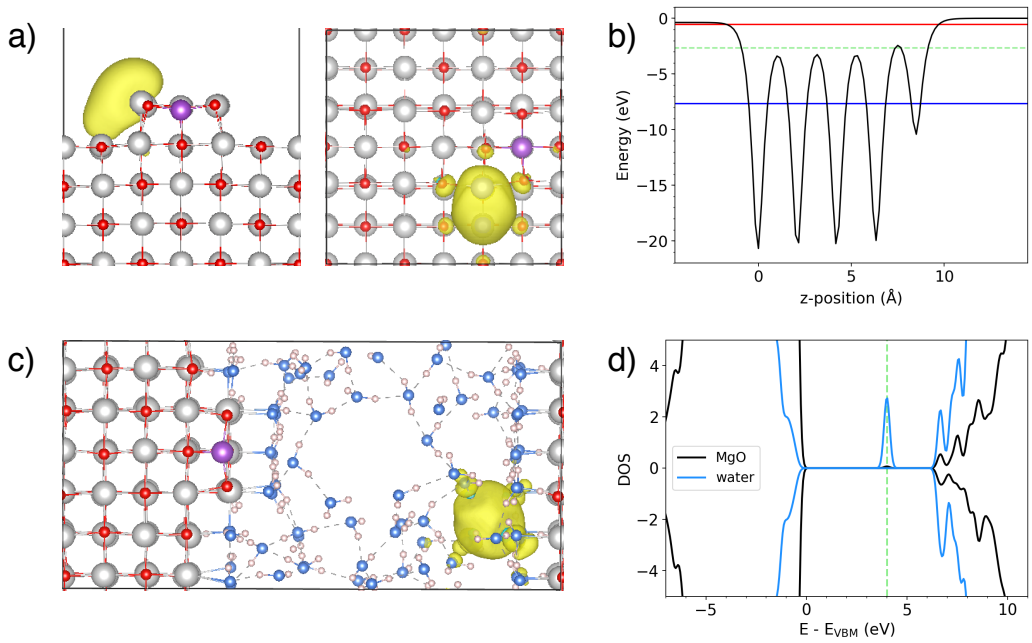


Figure 1: (a) "Stepped surface" model of Al-doped MgO(001) in vacuum (side and top views), and (b) corresponding potential energy profile along the direction ($z$) perpendicular to the surface; the horizontal lines indicate valence band maximum (VBM, blue), conduction band minimum (CBM, red), and energy level of the excess electron (DS, green). A dipole correction in the vacuum region is used to compensate the work function difference of 0.37 eV between the two sides of the slab. (c) Snapshot of the Al-doped MgO-water interface and (d) electronic density of states (DOS) of MgO (black line) and water (blue line) at the interface; the vertical green line indicates the Fermi level. The yellow iso-surfaces in (a) and (c) depict the spin density associated with the excess electron; the iso-surface value is 0.0011 a.u.. The atoms are color coded: Mg (grey), $O_s$ (red), $O_w$ (blue) and Al (purple).

The computed electronic structure of the Al-doped surface in vacuum (Figure 1b) is characterized by a band gap of 7.13 eV and a singly-occupied defect state (DS) at -2.12 eV relative to the CBM (or -2.65 eV vs. vacuum). As shown by the spin density contour in Figure 1a, and consistent with previous studies,[37] this state corresponds to an electron that is centered at the step edge and protrudes significantly toward the vacuum. A different structure is observed at the aqueous interface (Figure 1c): the excess electron, denoted $e^-_{surf,eq}$ to stress the equilibrium structure, is now localized within the first hydration layer against the flat side of the slab and away from the Al dopant, indicating that at least partial electron transfer from the MgO surface to water has occurred. The large extent of solvation of $e^-_{surf,eq}$

is confirmed by the projected densities of states (PDOS) in Figure 1d, which shows that the defect state in the band gap consists mostly of water orbitals. The calculated PDOS also shows that the conduction and valence band edges of MgO and water are almost coincident, with a total band gap of $6.98 \pm 0.20$ eV, similar to that found for the doped stepped surface in vacuum (averages and rmsd are calculated over 36 snapshots along the AIMD trajectory). The energy level of $e^-_{surf,eq}$ is at $3.13 \pm 0.30$ eV below the CBM of water, and is thus stabilized by more than 1 eV with respect to the DS in vacuum and comparable to the reported level of 2.75 eV below the CBM for the s-like state of a solvated electron in bulk liquid water, $e^-_{aq}$.[33] We quantified the localization of $e^-_{surf,eq}$ by calculating the radius of gyration ($R_g$). We obtained $R_g = 3.96 \pm 0.12$ Å, indicating that $e^-_{surf,eq}$ is less localized than $e^-_{aq}$ in bulk water ($R_g = 2.49 \pm 0.12$ Å).[32,38] We also found that $e^-_{surf,eq}$ has an anisotropy close to zero, indicating a quasi spherical s-like state.

## Calculation of Activation Barriers to Interfacial Electron Transfer

To characterize the kinetics of radiation-induced ET from the MgO conduction band to a localized state at the interface or in solution, we employed a description based on Marcus theory within which the reactant corresponded to a state in the conduction band of MgO and the product corresponded to a localized state at the interface or in solution (see Scheme. 1). In the physical systems, this ET is stimulated by photoexcitation of an electron to the conduction band. As a computational proxy accessible to ground-state DFT methods, we replaced a Mg atom in near-equilibrium configurations of the pristine MgO-water interface with an Al atom, which introduced an excess electron instantaneously to the system. We then performed short (5 ps) AIMD trajectories of this now out-of-equilibrium system, which allowed the doped systems to equilibrate sufficiently. From each short AIMD trajectory we obtained the reaction free energy $\Delta G^0$ and reorganization energy $\lambda$ for the electron transfer reaction, from which we computed the corresponding activation barrier $\Delta G^\ddagger$ according to Marcus theory for nonadiabatic electron transfer in solution,[39,40]

$$\Delta G^{\ddagger} = \frac{(\Delta G^0 + \lambda)^2}{4\lambda} \tag{1}$$

To obtain statistically representative estimates of $\Delta G^0$ and $\lambda$, we conducted nine of these short, 5-ps AIMD runs, which are hereafter referred to as trajectories 1-9. The initial configurations for trajectories 1-9 were taken to be well-separated snapshots along the AIMD trajectory of the pristine (stepped) MgO-water interface. In these initial configurations, one of the surface Mg was replaced by an Al atom to achieve instantaneous doping at the same lattice site used for the equilibrium simulation of the doped interface (Figure 1c). All nine trajectories relaxed to near equilibrium within 5 ps following the instantaneous doping as shown in Fig. S6.

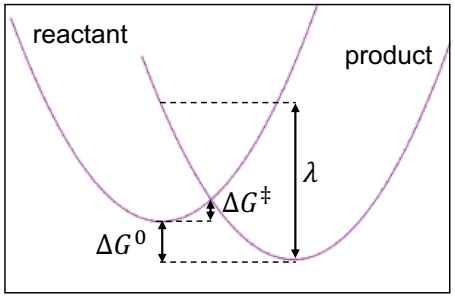


Scheme 1: Schematic of free energy parabolas along a collective solvent coordinate describing electron transfer from a delocalized conduction band (reactant) to a localized defect state (product). The reaction free energy ($\Delta G^0$), reorganization energy ($\lambda$), and activation energy $\Delta G^{\ddagger}$ are indicated by black arrows.

We estimated the reaction free energies $\Delta G^0$ for trajectories 1-9 as the difference in energy between the CBM at the initial configuration and the relevant defect state (DS) eigenvalue following equilibration. To do this, we performed single-point energy calculations on the initial and final snapshots of trajectories 1-9 and calculated the reaction free energy as:

$$\Delta G^0 = E_{DS,final} - E_{CBM} \tag{2}$$

where $E_{DS,final}$ and $E_{CBM}$ are the computed energy eigenvalues associated with the lo-

calized product DS and the MgO CBM, respectively. We estimated $\lambda$ as the total energy difference between the initial, instantaneously doped and the final, equilibrated configurations[20]

$$\lambda = E_{tot,initial} - \bar{E}_{tot,final} \tag{3}$$

where $E_{tot,initial}$ is the total energy of the initial configuration at the moment of doping and $\bar{E}_{tot,final}$ is the average of the total energy over the last 1 ps of the trajectory. From these $\Delta G^0$ and $\lambda$, we calculate the activation free energies of electron transfer for each trajectory according to Eq. 1. We justify using a nonadiabatic expression for the activation barrier to ET on the basis of the suspected small electronic coupling between delocalized states in the conduction band of the material and localized product electronic states translocated to the interface or solution.[41,42] While we cannot rule out that in the physical systems the radiation-induced ET may occur via hot carrier dynamics to which nonadiabatic rate theory would not apply, this framework allows for a quantitative analysis of the trajectories and comparison of different pathways.

## Two Pathways for Electron Transfer: $\mathbf{e^-_{surf}}$ and $\mathbf{H^\bullet}$

Two distinct pathways for electron transfer emerged from the out-of-equilibrium trajectories, one leading to formation of a surface solvated electron, $e^-_{surf}$ (trajectories 1-5), and the other to formation of a hydrogen radical species, $H^\bullet$ (trajectories 6-9).

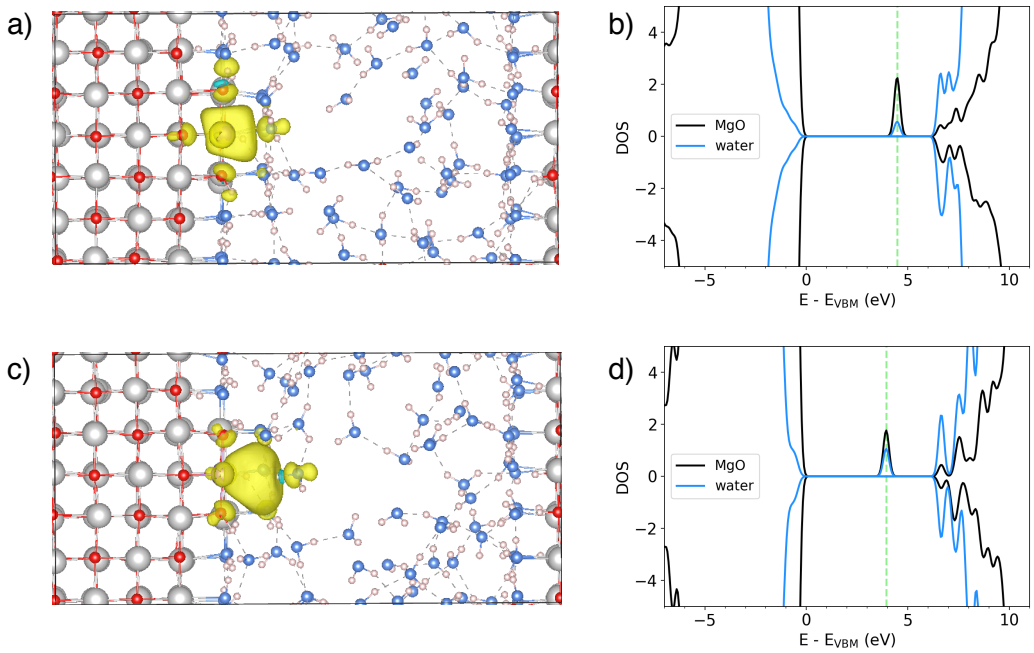


Figure 2: Snapshots of the doped MgO-water interface at initial (a) and final (c) time points of trajectory 1 that corresponds to the $e^-_{surf}$ pathway. Initial refers to the moment of instantaneous doping and and final refers to following 5 ps of AIMD equilibration. The yellow isosurfaces in (a) and (c) correspond to spin densities associated with the excess electron. (b) and (d) are the corresponding PDOS of MgO (black line) and water (blue line) at the interface; the vertical green lines indicate the Fermi levels.

In the $e^-_{surf}$ pathway, the excess electron is initially localized in an oxide surface state centered on the Al atom (Figure 2a and b), but drifts outward and becomes increasingly hydrated as the system equilibrates (Figure 2c). This also leads to a stabilization of the DS energy level in the band gap, which is found at $3.22 \pm 0.49$ eV below the CBM of water after 5 ps equilibration (Figure 2d), a similar energy to that of the excess electron at the equilibrated interface of doped MgO with water in Figure 1d. The computed values in Table 1 indicate small activation barriers to electron transfer via the $e^-_{surf}$ pathway. The computed solvent reorganization energies $\lambda$ and free energies of electron transfer $\Delta G^0$ are comparable in magnitude with opposite signs, despite the large variance among the computed $\lambda$. This variance can be largely attributed to the small size of the investigated model system and our limited ability to sample its out-of-equilibrium configurations.

Solvated electrons have been experimentally observed at the interfaces of metals and amorphous ice,[43–45] but metal oxide/liquid interfaces are less well understood due to a lack of suitable experimental characterization tools for such systems.[46] Several computational studies have revealed that solvated electrons at aqueous interfaces of metal oxides can be stabilized by dangling hydrogen bonds at the surface.[28,47–49] Moreover, experiments have determined that surface solvated electrons' long lifetimes are attributed to the high barriers associated with rearranging dangling OH bonds.[50] The relative stability of the $e^-_{surf}$ observed here can therefore be attributed the abundance of dangling hydrogen bonds at the interface of MgO. While hydrated electrons are known to be active species in water radiolysis,[5–7] none of the $e^-_{surf}$ states in our trajectories further reacted within 5 ps.

As a second pathway to ET, we observed the formation of a solvated radical $H^\bullet$ originating from one of the protons of a surface hydroxyl adjacent to the Al dopant (dashed black circles in Figure 3a and c). The initial state for this pathway is characterized by a spin density (Figure 3a) qualitatively similar to that for the $e^-_{surf}$ pathway, however the energy level in the band gap was generally shallower, i.e. less than 1 eV below the CBM (see Figure 3b). In the subsequent equilibration dynamics, the spin density of the excess electron is found to become increasingly localized on the proton of a surface hydroxyl close to the Al atom, until the O-H bond of the hydroxyl eventually breaks. At this point the resulting proton and the accompanying excess electron leave the surface as an H atom, as illustrated by the spin density isosurface becoming nearly perfectly spherical (Figure 3c). While no defect states were present in the band gap after the 5 ps equilibration, a closer look at the PDOS revealed a state associated with the solvated $H^\bullet$ lying a few eV below the VBM of water (Figure 3 d). From this energy eigenvalue we can compute a $\Delta G^0$ for this pathway on the order of about -8 eV (see Table 1). The solvent reorganization energy for the $H^\bullet$ pathway is in the range $2 - 3.6$ eV, which is similar to that of the $e^-_{surf}$ pathway (Table 1). The extreme exoergicity and modest $\lambda$ values of the $H^\bullet$ pathway give way to large $\Delta G^\ddagger$ values, despite the formation

of a thermodynamically favorable product.

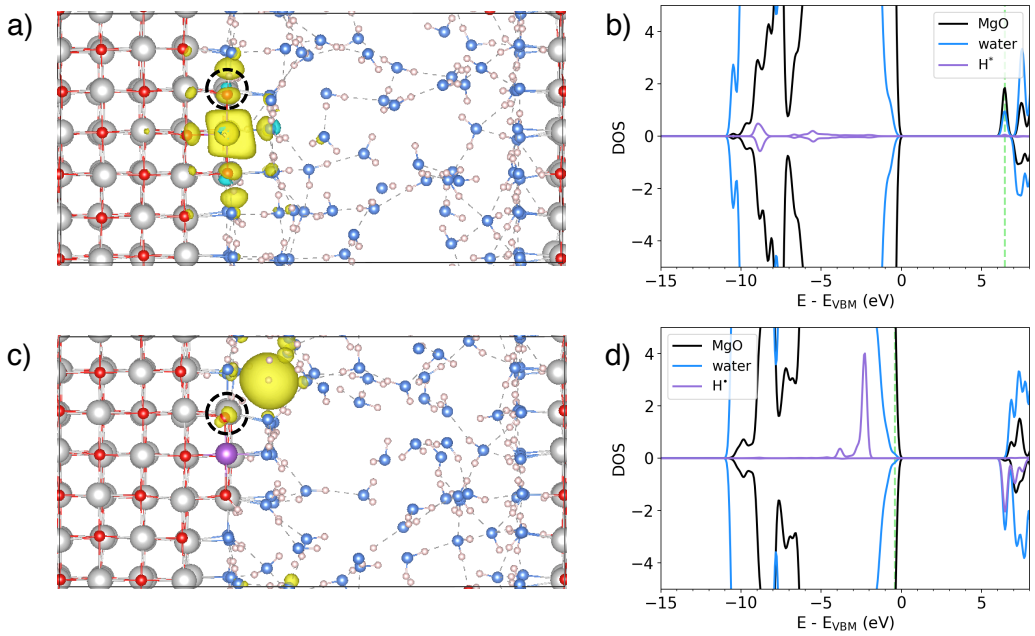


Figure 3: Snapshots of the doped MgO-water interface at initial (a) and final (c) times of trajectory 6 that are representative of the $H^{\bullet}$ pathway. Initial refers to the moment of instantaneous doping and and final refers to following 5 ps of AIMD equilibration. The yellow isosurfaces in (a) and (c) correspond to spin densities associated with the excess electron. The dashed black circles in (a) and (c) mark the location of the oxygen atom to which $H^{\bullet}$ is bound prior to radical formation. (b) and (d) are the corresponding PDOS of MgO (black line), water (blue line), and Al (purple) at the interface; the vertical green line indicates the Fermi level and the electronic state associated with $H^{\bullet}$ is below this level. The PDOS for $H^{\bullet}$ is multiplied by a factor of two for easier visualization.

Table 1: Solvent reorganization energies ($\lambda$), reaction free energies ($\Delta G^0$), and activation energies ($\Delta G^{\ddagger}$) of the electron transfer for both the $e^-_{surf}$ and $H^{\bullet}$ pathways. Starting configurations are taken from the AIMD trajectory of the pristine stepped (as) MgO-water interface. All quantities are in eV.

| $e^-_{surf}$ | $\lambda$ | $\Delta G^0$ | $\Delta G^{\ddagger}$ |
|---|---|---|---|
| | 3.39 | -3.17 | 0.004 |
| traj | 1.64 | -3.98 | 0.835 |
| 1 - 5 | 3.00 | -2.70 | 0.008 |
| | 2.24 | -3.54 | 0.189 |
| | 3.71 | -2.71 | 0.067 |
| $H^{\bullet}$ | | | |
| | 1.99 | -8.82 | 5.860 |
| traj | 3.59 | -8.72 | 1.833 |
| 6 - 9 | 2.80 | -7.52 | 1.989 |
| | 2.82 | -8.77 | 3.139 |

The formation of solvated $H^{\bullet}$ via the second pathway is reminiscent of the hydrogen loss reaction of $Mg^+(H_2O)_n$ ($5 < n < 15$) cluster ions, in which solvated electrons react with protons formed by $H_2O$ autoionization to form $H^{\bullet}$ species.[51] DFT calculations demonstrated that the hydrogen loss reaction is facilitated by the solvated electron's proximity to $H^+$ and the $OH^-$ species left behind is stabilized by direct coordination to the $Mg^{2+}$ ion.[51] We can identify analogous features in our trajectories that follow the $H^{\bullet}$ pathway. In fact, a solvated electron is initially localized either in the first hydration layer or on the Al atom, both of which are in close proximity of the departing proton. Moreover, the protons of surface hydroxyl groups adjacent to the Al dopant are indeed found to detach more easily because of the additional stabilization associated with coordinating to both $Al^{3+}$ and $Mg^{2+}$.

To further explore the role of the Al dopant's location in the formation of the ET products, we conducted two additional 5 ps AIMD runs where Al was not at the surface but in the interior of the MgO slab. These are denoted as trajectories 10 and 11 and are shown in greater detail in the SI. To control the number of variables, the initial configurations of trajectories 10 and 11 (other than the Al dopant) were the same as those of trajectories 1 ($e^-_{surf}$) and 6 ($H^{\bullet}$). Similarly to what was observed when Al is at the MgO surface, in

both the additional trajectories the excess electron is initially localized on the Al impurity (Figure S8a and b). As the system equilibrates, however, the excess electron migrates to within the first hydration layer on the flat side of the slab, qualitatively similar to the DS at the equilibrated aqueous interface of doped MgO (Figure 1c). Moreover, the computed solvent reorganization energies and free energies of electron transfer for trajectories 10 and 11 (Table S3) are comparable to those for trajectories 1-5 where the Al dopant sits right at the interface. These results thus suggest that the presence of the Al dopant at the surface may facilitate the formation of $H^{\bullet}$ species.

The characteristics of the $e^{-}_{surf}$ and $H^{\bullet}$ pathways are depicted schematically in Figure 4. The formation of $H^{\bullet}$ is thermodynamically favored as the reaction free energy is much more negative than that for the $e^{-}_{surf}$ pathway. In contrast, the formation of $e^{-}_{surf}$ is strongly kinetically favored compared to the formation of $H^{\bullet}$, given the much smaller calculated activation barriers. The computed differences in activation barriers for the two pathways is consistent with the experimental observation that hydrated electrons, rather than H radicals, are the main species responsible for $H_2$ formation in $\gamma$ radiolysis of water.[6,52,53]

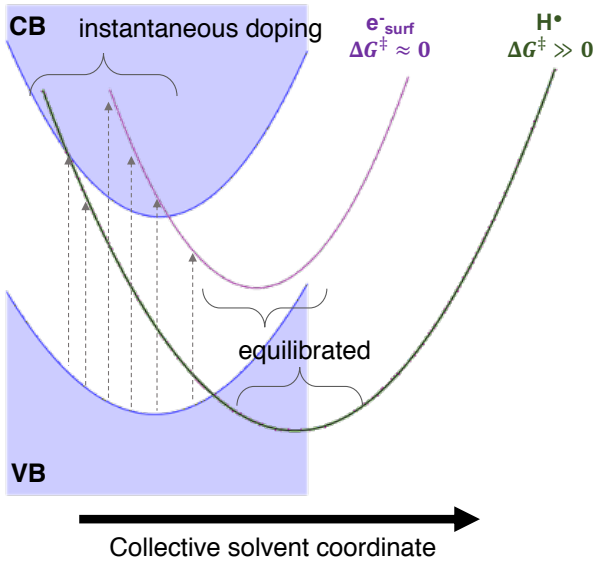


Figure 4: Schematic of the observed pathways of electron transfer from MgO to either an $e^-_{surf}$ or a hydrogen radical ($H^\bullet$). The VB and CB are depicted as quasi-continuous manifolds of electronic states separated by a band gap whereas the $e^-_{surf}$ and $H^\bullet$ product states are depicted as discrete. The vertical dashed arrows represent the creation of the out-of-equilibrium population of product states by instantaneous doping of various configurations at the MgO-water interface. This diagram shows that the $e^-_{surf}$ pathway has a small activation barrier and is thus kinetically favored, whereas the $H^\bullet$ pathway has a large barrier even though it is thermodynamically favorable.

We conducted further analyses to identify possible criteria for ET to occur via one pathway or another. Despite a slight trend towards higher DS energy levels at t = 0 ps for the $H^\bullet$ pathway trajectories, this trend is not definitive as we see overlap between trajectories associated with both pathways (see Figure S7). Furthermore, although the $H^\bullet$ pathway features very high activation barriers, the energies associated with the excess electron at t = 0 are comparable if not higher than the computed barriers. Lastly, the trajectories in which Al in the interior of the slab highlighted that Al doping on the surface was not required for the excess electron to localize at the interface. In the end, we can only ascribe the ET product to the femtosecond solvation dynamics of interfacial water following photoexcitation.[54,55]

# Conclusions

We investigated the equilibrium and out equilibrium behavior of excess electrons at the aqueous interface of wide gap oxide MgO using *ab initio* simulations where the excess electron was introduced via Al doping of the MgO slab. The equilibrium simulations revealed the excess electron to be localized in the interfacial hydration layer far from the Al impurity indicating (at least partial) electron transfer from the oxide to water across the interface. Both the energy (2.12 eV below the conduction band edge) and shape of this solvated electron are similar to literature characterizations of the hydrated electron in bulk water.

We then performed several short AIMD trajectories where the initial state was generated by introducing an Al dopant in a near-equilibrium configuration of the pristine MgO-water interface. The equilibration of these instantaneously out-of-equilibrium systems were used as a proxy to study the kinetics of the ET from the CB of MgO to product states at the interface and in solution. We observed two distinct products associated with the ET: a solvated electron similar to the one observed in the equilibrium simulation, denoted $e^-_{surf}$, and a H radical, denoted $H^\bullet$. The $e^-_{surf}$ pathway was characterized by an exoergic $\Delta G^0$ of about -3 eV and a $\lambda$ of about the same magnitude, yielding small $\Delta G^\ddagger$ values in the context of Marcus theory. The $H^\bullet$ pathway featured the cleavage of a surface hydroxyl moiety and the ultimate localization of the excess electron on an H atom in solution. The energy associated with this state was below the VBM, yielding very exoergic $\Delta G^0$ values of about -8 eV for this pathway. Given that the computed $\lambda$ for this pathway were comparable to those of the $e^-_{surf}$ pathway, the resulting $\Delta G^\ddagger$ for this pathway was very large, $\sim$3 eV.

These results provide context for the poor utility of MgO for stimulating water radiolysis.[4,6] The formation of a radical $H^\bullet$ species in solution, which we expect to further react to form $H_2$, carries a prohibitively high activation barrier. Conversely, the kinetic product for ET from the CB of MgO, the $e^-_{surf}$ species, remained local to the surface for the du-

ration of each trajectory in which it was observed. Given the favorable electron solvation environment provided by the high density hydration layer on the MgO surface, we speculate that the $e^-_{surf}$ species will remain close to the interface also on longer time scales, and thus this is likely an ineffective pathway for $H_2$ production. Taken together, the large barrier for the productive pathway and very small barrier to a putatively non-productive pathway is consistent with the negligible enhancement of the radiolytic yield of $H_2$ on MgO versus bulk water.[4,6] Moreover, we anticipate that the computational framework employed here will be broadly applicable to assessing ET mechanisms at aqueous, photocatalytic interfaces.

# Associated content

**Supporting Information:** Computational methodology, pristine and Al-doped MgO (001) surfaces in vacuum, equilibrium properties of MgO-water interfaces, additional information for trajectories 1-9, trajectories 10-11.

# Author Information

**Corresponding Author** AS email: aselloni@princeton.edu

# Acknowledgement

This work was supported by DoE-BES, Division of Chemical Sciences, Geosciences and Biosciences under Award DE-SC0007347. We also acknowledge support from the Computational Chemical Center: Chemistry in Solution and at Interfaces, funded by the DoE under Award DE-SC0019394. We used resources of the National Energy Research Scientifc Computing Center (DoE Contract No. DE-AC02- 05cH11231). We also acknowledge use of the TIGRESS High Performance Computer Center at Princeton University.

# References


(1) Linsebigler, A. L.; Lu, G.; Yates, J. T. Photocatalysis on TiO2 Surfaces: Principles, Mechanisms, and Selected Results. *Chemical Reviews* **1995**, *95*, 735–758.

(2) Fujishima, A.; Zhang, X.; Tryk, D. A. TiO2 photocatalysis and related surface phenomena. *Surface Science Reports* **2008**, *63*, 515–582.

(3) Schatz, T.; Cook, A. R.; Meisel, D. Charge Carrier Transfer across the Silica Nanoparticle/Water Interface. *The Journal of Physical Chemistry B* **1998**, *102*, 7225–7230.

(4) Petrik, N. G.; Alexandrov, A. B.; Vall, A. I. Interfacial Energy Transfer during Gamma Radiolysis of Water on the Surface of ZrO2 and Some Other Oxides. *J. Phys. Chem. B* **2001**, *105*, 5935–5944.

(5) Garrett, B. C. et al. Role of Water in Electron-Initiated Processes and Radical Chemistry:,Äâ Issues and Scientific Advances. *Chemical Reviews* **2005**, *105*, 355–390.

(6) Le Caër, S. Water Radiolysis: Influence of Oxide Surfaces on H2 Production under Ionizing Radiation. *Water* **2011**, *3*, 235–253.

(7) McGrady, J.; Yamashita, S.; Kano, S.; Yang, H.; Kimura, A.; Abe, H. H2 generation at metal oxide particle surfaces under $\gamma$-radiation in water. *Journal of Nuclear Science and Technology* **2021**, *58*, 604–609.

(8) Chelnokov, E.; Cuba, V.; Simeone, D.; Guigner, J.-M.; Schmidhammer, U.; Mostafavi, M.; Le Caër, S. Electron Transfer at Oxide/Water Interfaces Induced by Ionizing Radiation. *The Journal of Physical Chemistry C* **2014**, *118*, 7865–7873.

(9) McGrady, J.; Yamashita, S.; Kano, S.; Yang, H.; Abe, H. Charge transfer across the Cr2O3, Fe2O3, and ZrO2 oxide/water interface: A pulse radiolysis study. *Radiation Physics and Chemistry* **2021**, *180*, 109240.

(10) Svoboda, V.; Michiels, R.; LaForge, A. C.; Med, J.; Stienkemeier, F.; Slavíček, P.; Wörner, H. J. Real-time observation of water radiolysis and hydrated electron formation induced by extreme-ultraviolet pulses. *Science Advances* **2020**, *6*, eaaz0385.

(11) Kerisit, S. N.; Shen, Z.; Prange, M. P.; Ilton, E. S. Separation of Radiolytic Species at the Boehmite–Water Interface. *The Journal of Physical Chemistry C* **2019**, *123*, 15534–15539.

(12) Sassi, M.; Walter, E. D.; Qafoku, O.; Rosso, K. M.; Wang, Z. Radiation-induced interfacial hydroxyl transformation on boehmite and gibbsite basal surfaces. *The Journal of Physical Chemistry C* **2020**, *124*, 22185–22191.

(13) Laporte, S.; Finocchi, F.; Paulatto, L.; Blanchard, M.; Balan, E.; Guyot, F.; Saitta, A. M. Strong electric fields at a prototypical oxide/water interface probed by ab initio molecular dynamics: MgO(001). *Phys. Chem. Chem. Phys.* **2015**, *17*, 20382–20390.

(14) Ding, Z.; Selloni, A. Hydration structure of flat and stepped MgO surfaces. *The Journal of Chemical Physics* **2021**, *154*, 114708.

(15) Adhikari, N. M.; Tuladhar, A.; Wang, Z.; De Yoreo, J. J.; Rosso, K. M. No Hydrogen Bonding between Water and Hydrophilic Single Crystal MgO Surfaces? *The Journal of Physical Chemistry C* **2021**, *125*, 26132–26138.

(16) Yang, J.; Youssef, M.; Yildiz, B. Structure, Kinetics, and Thermodynamics of Water and Its Ions at the Interface with Monoclinic ZrO2 Resolved via Ab Initio Molecular Dynamics. *The Journal of Physical Chemistry C* **2021**, *125*, 15233–15242.

(17) Akimov, A. V.; Neukirch, A. J.; Prezhdo, O. V. Theoretical Insights into Photoinduced Charge Transfer and Catalysis at Oxide Interfaces. *Chemical Reviews* **2013**, *113*, 4496–4565.

(18) Chen, J.; Li, Y.-F.; Sit, P.; Selloni, A. Chemical Dynamics of the First Proton-Coupled Electron Transfer of Water Oxidation on TiO2 Anatase. *JOURNAL OF THE AMERICAN CHEMICAL SOCIETY* **2013**, *135*, 18774–18777.

(19) Akimov, A. V.; Muckerman, J. T.; Prezhdo, O. V. Nonadiabatic Dynamics of Positive Charge during Photocatalytic Water Splitting on GaN(10-10) Surface: Charge Localization Governs Splitting Efficiency. *JOURNAL OF THE AMERICAN CHEMICAL SOCIETY* **2013**, *135*, 8682–8691.

(20) Cheng, J.; VandeVondele, J.; Sprik, M. Identifying Trapped Electronic Holes at the Aqueous TiO2 Interface. *The Journal of Physical Chemistry C* **2014**, *118*, 5437–5444.

(21) Ertem, M. Z.; Kharche, N.; Batista, V. S.; Hybertsen, M. S.; Tully, J. C.; Muckerman, J. T. Photoinduced Water Oxidation at the Aqueous GaN (10(1)over-bar0) Interface: Deprotonation Kinetics of the First Proton-Coupled Electron-Transfer Step. *ACS CATALYSIS* **2015**, *5*, 2317–2323.

(22) Li, Y.-F.; Selloni, A. Pathway of Photocatalytic Oxygen Evolution on Aqueous TiO2 Anatase and Insights into the Different Activities of Anatase and Rutile. *ACS Catalysis* **2016**, *6*, 4769–4774.

(23) Gono, P.; Ambrosio, F.; Pasquarello, A. Effect of the Solvent on the Oxygen Evolution Reaction at the TiO2-Water Interface. *JOURNAL OF PHYSICAL CHEMISTRY C* **2019**, *123*, 18467–18474.

(24) Hammes-Schiffer, S.; Galli, G. Integration of theory and experiment in the modelling of heterogeneous electrocatalysis. *NATURE ENERGY* **2021**, *6*, 700–705.

(25) Warburton, R. E.; Mayer, J. M.; Hammes-Schiffer, S. Proton-Coupled Defects Impact O-H Bond Dissociation Free Energies on Metal Oxide Surfaces. *JOURNAL OF PHYSICAL CHEMISTRY LETTERS* **2021**, *12*, 9761–9767.

(26) Rousseau, R.; Glezakou, V.-A.; Selloni, A. Theoretical insights into the surface physics and chemistry of redox-active oxides. *Nature Reviews Materials* **2020**, *5*, 460–475.

(27) Pacchioni, G.; Freund, H. Electron Transfer at Oxide Surfaces. The MgO Paradigm: from Defects to Ultrathin Films. *Chemical Reviews* **2013**, *113*, 4035–4072, PMID: 23116191.

(28) Selcuk, S.; Selloni, A. Facet-dependent trapping and dynamics of excess electrons at anatase TiO2 surfaces and aqueous interfaces. *Nature Materials* **2016**, *15*, 1107–1112.

(29) Mori-Sanchez, P.; Cohen, A. J.; Yang, W. Many-electron self-interaction error in approximate density functionals. *The Journal of Chemical Physics* **2006**, *125*, 201102.

(30) Vargas, J.; Ufondu, P.; Baruah, T.; Yamamoto, Y.; Jackson, K. A.; Zope, R. R. Importance of self-interaction-error removal in density functional calculations on water cluster anions. *Phys. Chem. Chem. Phys.* **2020**, *22*, 3789–3799.

(31) Yamijala, S. S. R. K. C.; Shinde, R.; Wong, B. M. Real-time degradation dynamics of hydrated per- and polyfluoroalkyl substances (PFASs) in the presence of excess electrons. *Phys. Chem. Chem. Phys.* **2020**, *22*, 6804–6808.

(32) Ambrosio, F.; Miceli, G.; Pasquarello, A. Electronic Levels of Excess Electrons in Liquid Water. *The Journal of Physical Chemistry Letters* **2017**, *8*, 2055–2059, PMID: 28407469.

(33) Pizzochero, M.; Ambrosio, F.; Pasquarello, A. Picture of the wet electron: a localized transient state in liquid water. *Chem. Sci.* **2019**, *10*, 7442–7448.

(34) Franchini, C.; Reticcioli, M.; Setvin, M.; Diebold, U. Polarons in materials. *Nature Reviews Materials* **2021**, *6*, 560–586.

(35) Björneholm, O.; Hansen, M. H.; Hodgson, A.; Liu, L.-M.; Limmer, D. T.; Michaelides, A.; Pedevilla, P.; Rossmeisl, J.; Shen, H.; Tocci, G.; Tyrode, E.; Walz, M.-

M.; Werner, J.; Bluhm, H. Water at Interfaces. *Chemical Reviews* **2016**, *116*, 7698–7726, PMID: 27232062.

(36) Włodarczyk, R.; Sierka, M.; Kwapień, K.; Sauer, J.; Carrasco, E.; Aumer, A.; Gomes, J. F.; Sterrer, M.; Freund, H.-J. Structures of the Ordered Water Monolayer on MgO(001). *The Journal of Physical Chemistry C* **2011**, *115*, 6764–6774.

(37) McKenna, K. P.; Sushko, P. V.; Shluger, A. L. Inside Powders: A Theoretical Model of Interfaces between MgO Nanocrystallites. *Journal of the American Chemical Society* **2007**, *129*, 8600–8608, PMID: 17569535.

(38) Uhlig, F.; Marsalek, O.; Jungwirth, P. Unraveling the Complex Nature of the Hydrated Electron. *The Journal of Physical Chemistry Letters* **2012**, *3*, 3071–3075, PMID: 26292252.

(39) Marcus, R. A. Chemical and electrochemical electron-transfer theory. *Annual review of physical chemistry* **1964**, *15*, 155–196.

(40) Marcus, R. A.; Sutin, N. Electron transfers in chemistry and biology. *Biochimica et Biophysica Acta (BBA)-Reviews on Bioenergetics* **1985**, *811*, 265–322.

(41) Kondov, I.; Čížek, M.; Benesch, C.; Wang, H.; Thoss, M. Quantum Dynamics of Photoinduced Electron-Transfer Reactions in Dye- Semiconductor Systems: First-Principles Description and Application to Coumarin 343- TiO2. *The Journal of Physical Chemistry C* **2007**, *111*, 11970–11981.

(42) Ghosh, S.; Castillo-Lora, J.; Soudackov, A. V.; Mayer, J. M.; Hammes-Schiffer, S. Theoretical insights into proton-coupled electron transfer from a photoreduced ZnO nanocrystal to an organic radical. *Nano letters* **2017**, *17*, 5762–5767.

(43) Gahl, C.; Bovensiepen, U.; Frischkorn, C.; Wolf, M. Ultrafast Dynamics of Electron Localization and Solvation in Ice Layers on Cu(111). *Phys. Rev. Lett.* **2002**, *89*, 107402.

(44) Stähler, J.; Gahl, C.; Bovensiepen, U.; Wolf, M. Ultrafast Electron Dynamics at Ice-Metal Interfaces: Competition between Heterogeneous Electron Transfer and Solvation. *The Journal of Physical Chemistry B* **2006**, *110*, 9637–9644, PMID: 16686513.

(45) Stähler, J.; Deinert, J.-C.; Wegkamp, D.; Hagen, S.; Wolf, M. Real-Time Measurement of the Vertical Binding Energy during the Birth of a Solvated Electron. *Journal of the American Chemical Society* **2015**, *137*, 3520–3524, PMID: 25611976.

(46) Lapointe, F.; Wolf, M.; Campen, R. K.; Tong, Y. Probing the Birth and Ultrafast Dynamics of Hydrated Electrons at the Gold/Liquid Water Interface via an Optoelectronic Approach. *Journal of the American Chemical Society* **2020**, *142*, 18619–18627, PMID: 32954719.

(47) Zhao, J.; Li, B.; Jordan, K. D.; Yang, J.; Petek, H. Interplay between hydrogen bonding and electron solvation on hydrated $TiO_2$(110). *Phys. Rev. B* **2006**, *73*, 195309.

(48) Zhao, J.; Yang, J.; Petek, H. Theoretical study of the molecular and electronic structure of methanol on a $TiO_2$(110) surface. *Phys. Rev. B* **2009**, *80*, 235416.

(49) Wang, Y.; Guo, H.; Zheng, Q.; Saidi, W. A.; Zhao, J. Tuning Solvated Electrons by Polar–Nonpolar Oxide Heterostructure. *The Journal of Physical Chemistry Letters* **2018**, *9*, 3049–3056, PMID: 29767527.

(50) Siefermann, K. R.; Liu, Y.; Lugovoy, E.; Link, O.; Faubel, M.; Buck, U.; Winter, B.; Abel, B. Binding energies, lifetimes and implications of bulk and interface solvated electrons in water. *Nature chemistry* **2010**, *2*, 274–279.

(51) Siu, C.-K.; Liu, Z.-F. Reaction mechanisms for size-dependent H loss in Mg+(H2O)n: solvation controlled electron transfer. *Phys. Chem. Chem. Phys.* **2005**, *7*, 1005–1013.

(52) Pastina, B.; LaVerne, J. A.; Pimblott, S. M. Dependence of Molecular Hydrogen For-

mation in Water on Scavengers of the Precursor to the Hydrated Electron. *The Journal of Physical Chemistry A* **1999**, *103*, 5841–5846.

(53) LaVerne, J. A.; Pimblott, S. M. New Mechanism for H2 Formation in Water. *The Journal of Physical Chemistry A* **2000**, *104*, 9820–9822.

(54) Jimenez, R.; Fleming, G. R.; Kumar, P.; Maroncelli, M. Femtosecond solvation dynamics of water. *Nature* **1994**, *369*, 471–473.

(55) Zimdars, D.; Dadap, J. I.; Eisenthal, K. B.; Heinz, T. F. Femtosecond dynamics of solvation at the air/water interface. *Chemical physics letters* **1999**, *301*, 112–120.

# TOC Graphic